

See discussions, stats, and author profiles for this publication at: <https://www.researchgate.net/publication/6156662>

DNA and Protein Footprinting Analysis of the Modulation of DNA Binding by the N-Terminal Domain of the *Saccharomyces cerevisiae* TATA Binding Protein

ARTICLE in BIOCHEMISTRY · OCTOBER 2007

Impact Factor: 3.02 · DOI: 10.1021/bi7003608 · Source: PubMed

CITATIONS

17

READS

19

8 AUTHORS, INCLUDING:



Huiyong Cheng

Albert Einstein College of Medicine

10 PUBLICATIONS 100 CITATIONS

SEE PROFILE



Sergei Khrapunov

Albert Einstein College of Medicine

85 PUBLICATIONS 352 CITATIONS

SEE PROFILE

DNA and Protein Footprinting Analysis of the Modulation of DNA Binding by the N-Terminal Domain of the *Saccharomyces cerevisiae* TATA Binding Protein

Sayan Gupta,^{‡,§,||} Huiyong Cheng,^{‡,⊥} A. K. M. M. Mollah,[#] Elizabeth Jamison,[⊥] Stephanie Morris,[⊥] Mark R. Chance,^{§,||} Sergei Khrapunov,^{*,⊥} and Michael Brenowitz^{*,§,⊥}

Department of Biochemistry, Albert Einstein College of Medicine, 1300 Morris Park Avenue, Bronx, New York 10461, Department of Biology, Yeshiva University, 500 West 185th Street, New York, New York 10033, Center for Proteomics, Case Western Reserve University, 10900 Euclid Avenue, Cleveland, Ohio 44106, and Center for Synchrotron Biosciences, National Synchrotron Light Source, Brookhaven National Laboratory, Upton, New York 11973

Received February 21, 2007; Revised Manuscript Received May 30, 2007

ABSTRACT: Recombinant full-length *Saccharomyces cerevisiae* TATA binding protein (TBP) and its isolated C-terminal conserved core domain (TBPc) were prepared with measured high specific DNA-binding activities. Direct, quantitative comparison of TATA box binding by TBP and TBPc reveals greater affinity by TBPc for either of two high-affinity sequences at several different experimental conditions. TBPc associates more rapidly than TBP to TATA box bearing DNA and dissociates more slowly. The structural origins of the thermodynamic and kinetic effects of the N-terminal domain on DNA binding by TBP were explored in comparative studies of TBPc and TBP by “protein footprinting” with hydroxyl radical ($\cdot\text{OH}$) side chain oxidation. Some residues within TBPc and the C-terminal domain of TBP are comparably protected by DNA, consistent with solvent accessibility changes calculated from core domain crystal structures. In contrast, the reactivity of some residues located on the top surface and the DNA-binding saddle of the C-terminal domain differs between TBP and TBPc in both the presence and absence of bound DNA; these results are not predicted from the crystal structures. A strikingly different pattern of side chain oxidation is observed for TBP when a nonionic detergent is present. Taken together, these results are consistent with the N-terminal domain actively modulating TATA box binding by TBP and nonionic detergent modulating the interdomain interaction.

The TATA binding protein (TBP)¹ is required for the initiation of transcription by each of the three eukaryotic RNA polymerases (*1*). TBP is composed of two domains. The C-terminal domain (TBPc) is highly conserved and binds TATA box sequences with high affinity and specificity. In contrast, the N-terminal domain of TBP is highly variable species to species with regard to both its primary sequence and length (*2*). Except for the TBP of *Arabidopsis thaliana* that has a rudimentary N-terminal domain, crystallographic studies of both free and DNA-bound protein have been carried out using TBPc (*3–12*). Published biochemical studies have been carried out using either full-length TBP or TBPc.

The general view of the N-terminal domain is that it is dynamic and minimally structured (*13–15*). Differences in DNA binding by TBP and TBPc in vitro have been described including enhanced binding affinity and DNA bending when the N-terminal residues are not present (*16, 17*). It was proposed that conformational changes involving the N-terminal domain might contribute to isomerization steps during the formation of a stable TBP–DNA complex and that the natural conformation of TBP is not optimal for DNA binding (*16, 17*). Evidence for the interaction of the N-terminal domain with the DNA-binding “saddle” and its displacement by DNA is indicated by intrinsic protein fluorescence and protein footprinting (*13, 18*).

The diminished affinity of human TBP relative to its isolated core domain suggests that the N-terminal domain inhibits DNA binding by the protein’s C-terminal domain (*19*). However, comparisons between TBP and TBPc have been done without determination of the specific DNA-binding activity of protein preparations, leaving ambiguous whether these are true differences. An additional complication is that both proteins self-associate. TBP follows a monomer–tetramer–octamer assembly pathway while TBPc dimerizes (*14, 20–22*). TBP oligomers rapidly reequilibrate in the presence of DNA ligand (*23*) while TBPc dimers slowly dissociate under some experimental conditions (*20, 24*). The N-terminal domain mediates the self-assembly reaction of the full-length protein (*14, 25*).

* To whom correspondence may be addressed. M.B.: e-mail, brenowit@aecom.yu.edu; phone, (718) 430-3179; fax, (718) 430-8565. S.K.: e-mail, khraps@aecom.yu.edu; phone, (718) 430-3180; fax, (718) 430-8565.

[‡]These authors contributed equivalently to this study.

[§] Brookhaven National Laboratory.

^{||} Case Western Reserve University.

[⊥] Albert Einstein College of Medicine.

[#] Yeshiva University.

¹ Abbreviations: TBP, TATA binding protein; TBPc, DNA-binding domain of TATA binding protein; AdMLP, adenovirus major late promoter; Brij, nonionic detergent Brij-58; DTT, redox reagent dithiothreitol; HPLC, high-pressure liquid chromatography; ESI, electrospray ionization; MS/MS, tandem mass spectrometry; $\cdot\text{OH}$, hydroxyl radical; CV, column volume; bp, base pair.

This study compares the equilibrium binding and association and dissociation kinetics of TBP and TBPc preparations whose specific DNA binding activities have been quantitated. These data clearly show that the N-terminal domain reduces the affinity of the C-terminal core for TATA box bearing DNA. The decreased affinity is the result of both decreased association and increased dissociation rates. Insight into the structure of the N-terminal domain, its interaction with the C-terminal core domain, and the changes that occur upon the binding of DNA has been obtained by comparative protein footprinting of TBP and TBPc that extend earlier work conducted only on the full-length protein (18). The role of this autoinhibitory interaction in regulating transcription initiation is discussed.

EXPERIMENTAL PROCEDURES

Materials

Protein Expression and Purification. The standard expression and purification protocols for TBP and TBPc (26–28) were modified to improve their yields and specific DNA-binding activities. The *Saccharomyces cerevisiae* TBP gene SPT 15 was cloned into the pET15b expression vector and expressed in *Escherichia coli* BL21(DE3) pLysS to produce TBP with a His tag affixed to the N-terminus (R. Moir, personal communication). Similarly, expression of plasmid p5J-yTBPc in *E. coli* strain BL21(DE3) produced *S. cerevisiae* TBPc with a His tag attached to the N-terminus (8). TBPc begins at residue 61 of TBP. Cells lines were streaked on LB agar plates containing 50 $\mu\text{g}/\text{mL}$ ampicillin and 34 $\mu\text{g}/\text{mL}$ chloramphenicol for TBPc and TBP, respectively, and incubated overnight at 37 °C. Colonies scrubbed from a single plate were resuspended in 1.0 mL of YT broth. Resuspended cells were used to inoculate 500 mL YT broths either containing 2% sucrose and 100 $\mu\text{g}/\text{mL}$ ampicillin or containing 0.4% glucose, 100 $\mu\text{g}/\text{mL}$ ampicillin, and 34 $\mu\text{g}/\text{mL}$ chloramphenicol for TBPc and TBP, respectively. Cells were grown at 37 °C until the OD of the cell suspensions became ~ 0.6 – 0.8 . IPTG was added to a final concentration of 1 mM to induce protein expression. Cells were further incubated at 37 °C for 2 h and then harvested at 3000g for 20 min at 4 °C. The cell pellet was washed once with buffer A (40 mM HEPES–NaOH, pH 7.9, 20% glycerol, 500 mM KCl, 5 mM imidazole, and 2 mM MgCl_2) and stored at -80 °C.

The same purification protocol is used for TBP and TBPc unless otherwise noted. All steps are carried out at 4 °C unless otherwise noted. Frozen cells were thawed on ice and resuspended at 5 mL/g in buffer A containing complete protease inhibitor cocktail tablets (Roche catalog no. 1873580). The cell suspension surrounded by a jacket filled with ice–water saturated with NaCl was lysed by sonication with 30 s bursts spaced 2 min apart. The cell lysate was centrifuged in a Sorvall SS-34 rotor at 11000 rpm for 20 min. Chromosomal DNA was precipitated from the supernatant by dropwise addition of 10% protamine (2.5 mL/20 mL of sample; Sigma catalog no. P4505) along with gentle stirring for 10 min. The precipitate was removed by centrifugation as above, and the supernatant was processed through the following chromatographic steps.

An Econo-Pac disposable chromatography column (Bio-Rad catalog no. 732-1010) packed with 2 mL of Ni-NTA

agarose (Qiagen catalog no. 30120) was equilibrated with 10 column volumes of buffer A and set up for gravity flow. Following sample loading, the column was sequentially washed with 5 column volumes of buffer A, buffer B (40 mM HEPES–KOH, pH 7.9, 20% glycerol, 1 M KCl, 2 mM MgCl_2 , and 5 mM imidazole), and buffer C (40 mM HEPES–KOH, pH 7.9, 20% glycerol, 200 mM KCl, 2 mM MgCl_2 , and 20 mM imidazole). The TBP was eluted with 5 column volumes of buffer D (40 mM HEPES–KOH, pH 7.9, 10% glycerol, 200 mM KCl, 2 mM MgCl_2 , and 250 mM imidazole). The elute was mixed with thrombin to remove the His tag (10 units of thrombin/mg of sample; Amersham catalog no. 27-0846-01) and dialyzed (Spectrum Laboratories, tubing no. 132678) at 14 °C overnight against buffer E (25 mM HEPES–KOH, pH 7.9, 20% glycerol, 3 mM CaCl_2 , 2 mM MgCl_2 , and 100 mM KCl). KCl was added into the digestion product to 500 mM and the sample loaded on the regenerated Ni-NTA column. The TBP-containing flow-through was collected and dialyzed against buffer E overnight.

The cleaved peptide was removed with a 2 mL column of Q-Sepharose (Amersham catalog no. 17-1014-0) equilibrated with 10 column volumes of buffer E. The dialyzed solution was loaded on the column and the flow-through collected. The protein-containing solution was dialyzed overnight against buffer F (25 mM HEPES–KOH, pH 7.9, 20% glycerol, 1 mM EDTA, 1 mM DTT, and 300 mM KCl), concentrated by Centricon (Millipore catalog no. 4205), and stored in small aliquots at -70 °C.

DNA Preparation. Unlabeled DNA oligonucleotides were obtained from Invitrogen or TriLink Biotechnologies, Inc. Oligonucleotide concentration was determined using extinction coefficients calculated from the base pair composition (29). A 18 bp oligonucleotide duplex bearing the TATA box sequence of the adenovirus major late promoter (AdMLP) of the sequence 5'-CGCTATAAAAGGGCTGGG-3' was prepared; annealing titrations of the complement were conducted to ensure that all of the oligonucleotides present in binding assays were duplex. DNase I footprinting studies were carried out using a *Hind*III (^{32}P -labeled)/*Nde*I restriction fragment of 282 bp bearing the AdMLP prepared from plasmid ppUMLP (30, 31) or a *Hind*III (^{32}P -labeled)/*Bsr*DI restriction fragment of 204 bp bearing the yeast U6 promoter prepared from plasmid pM4 (32).

Methods

Analytical Ultracentrifugation. Sedimentation equilibrium studies were conducted at 20 and 22 °C using the absorption optics of a Beckman XL-I analytical centrifuge essentially as described previously (14, 21). The protein was dialyzed against pH 7.6 buffer containing either 25 mM cacodylic acid or Tris–HCl, 5 mM MgCl_2 , 1 mM CaCl_2 , 0.2 mM DTT, and 100 mM KCl with or without the nonionic detergent 0.01% Brij-58. The data were analyzed using the XL-A/XL-I analysis software (Beckman Instruments).

Absorption and Fluorescence Spectroscopy. Optical measurements were performed in buffer containing 25 mM Tris–HCl, 100 mM KCl, 5 mM MgCl_2 , 1 mM CaCl_2 , and 2 mM DTT at pH 7.5 and 22 °C. BSA (Sigma) at 50 $\mu\text{g}/\text{mL}$ was added to the solution when binding isotherms were measured using fluorescent labeled oligonucleotides. Absorption mea-

measurements were made using a Beckman Coulter DU 7400 spectrophotometer (Fullerton, CA). Fluorescence measurements were made using a Jobin Yvon Fluoromax-3 spectrofluorometer (Edison, NJ) corrected for the spectral sensitivity of the instruments.

Measurement of Extinction Coefficients and Determination of Specific DNA-Binding Activity. The concentration of the oligonucleotides and the proteins used in binding studies was determined from absorption measurement by using their respective extinction coefficients at specific wavelengths. The extinction coefficient at 260 nm for the 18 bp duplex DNA was estimated from the base pair composition as mentioned above (29). TBP and TBPC extinction coefficients were determined from $\epsilon_{M,nat} = Abs_{nat}/\epsilon_{M,Gdn}/Abs_{Gdn}$, where $\epsilon_{M,nat}$ and $\epsilon_{M,Gdn}$ are the extinction coefficients and Abs_{nat} and Abs_{Gdn} are the optical densities of the native and denatured protein in 6 M guanidine hydrochloride, respectively, at 278 nm (33). $\epsilon_{M,Gdn}$ is calculated from the number of aromatic amino acids and cysteine using the molar extinction coefficients for appropriate model compounds as reported earlier (34). The concentrations of TBP and TBPC were determined from the absorption measure at 278 nm by using the extinction coefficients 15180 and 9540 M⁻¹ cm⁻¹, respectively.

The specific DNA-binding activity was determined by titration of 0.5 μ M TBP or TBPC with increasing concentrations of the 18 bp DNA duplex in buffer containing 10 mM sodium cacodylate, 100 mM KCl, 5.0 mM MgCl₂, and 1.0 mM CaCl₂ at pH 7.6 and 22 °C. Since these protein concentrations were significantly greater than the K_d of the binding reaction, the titration resulted in a linear increase in complex concentration until an equivalence point was reached. The net change in the intrinsic fluorescence of TBP and TBPC upon binding the unlabeled DNA was used to calculate the fractional saturation of the protein (15). The ratio of the fluorescence emissions at 365 and 306 nm was used to quantitate DNA binding to TBP (15) while the intensity of fluorescence at 306 nm was used to quantitate DNA binding to TBPC. The excitation wavelength is 275 nm for both experiments. The equivalent point was determined by fitting the data to two intersecting lines. The fractional activity of the protein was determined from the intersection point assuming a 1:1 protein:DNA stoichiometry.

Equilibrium and Kinetic Quantitative Footprinting. Quantitative DNase I footprint titration experiments were conducted in solutions containing 100 mM KCl, 5.0 mM MgCl₂, 1.0 mM CaCl₂, and 50 μ g/mL BSA at pH 7.6 and 22 °C as described (30, 31, 35). The buffer used was either 25 mM sodium cacodylate, BisTris, Tris-HCl, or KH₂PO₄ as indicated. Isotherms were also determined in solutions additionally containing 0.01% Brij. The transition curves were scaled to fractional saturation and fit to the Hill equation as described elsewhere (35). The quench-flow DNase I kinetic footprinting experiments were conducted and analyzed as described (30, 31, 36, 37) in the solution described above with BisTris as the buffer. The resultant autoradiograms were digitized using a Storm imager and quantitated with ImageQuant (Molecular Dynamics) as described (37).

Protein •OH Footprinting. TBP, TBPC, and their binary complexes with the 18 bp DNA duplex were prepared to a final concentration of 1 μ M in 10 mM potassium phosphate buffer at pH 7.6 containing 100 mM KCl, 5 mM MgCl₂, 1

mM CaCl₂, 0.01% Brij, and 0.1 mM EDTA. Samples were also prepared in similar buffer omitting Brij and CaCl₂. The free protein and complex were exposed to white synchrotron light at the National Synchrotron Light Source's (Brookhaven National Laboratory, Upton, NY) beamline X-28C operating at a ring energy of 2.8 GeV (18, 38–40). The KinTek quench-flow mixer present at the beamline was modified so that a single syringe pushed sample from 50 or 250 μ L loops through the synchrotron beam. The flow rate of the sample was adjusted to control the exposure time by the KinTek controller software program PACCOM version 3.20 from Pacific Scientific Digital Motion Control Products. The continuous flow arrangement allowed large volumes of low concentration samples to be exposed to the X-ray beam for durations up to 120 ms. All sample exposures were conducted at room temperature. The exposed samples were collected in microfuge tubes containing methionine amide to quench the peroxide induced secondary oxidation during the postexposure sample handling time periods (41, 42). Samples were frozen in dry ice and stored in -80 °C.

Chromatography and Mass Spectrometry. The frozen samples were thawed, and trypsin (Promega) was added to an enzyme:protein ratio of 1:40 (w/w) in the presence of 10% acetonitrile and 0.1 μ M CaCl₂. The pH of the sample solution was maintained at pH 8.2 by the addition of ammonium carbonate buffer to a final concentration of 50 mM. The digestion reaction was carried out at 37 °C for 12 h. The digested peptides from samples exposed without the detergent Brij were introduced into a ThermoFinnigan LCQ classic mass spectrometer via a Waters Alliance 2690 high-pressure liquid chromatography system (ThermoFinnigan Inc., San Jose, CA; Waters Corp., Milford, MA). The reverse-phase chromatographic separations were performed with 200 pmol of digested proteins on a 1 \times 150 mm C18 column (Vydac Separations Group Inc., Hesperia, CA) at a flow rate of 50 μ L/min with a 2% gradient of acetonitrile and water containing 0.05% trifluoroacetic acid. The digested peptides from samples exposed with the detergent Brij were introduced into a ThermoFinnigan Deca XP Plus mass spectrometer equipped with a nanospray ion source, via an UltiMate nanoseparation reverse-phase HPLC system (ThermoFinnigan Inc., San Jose, CA; LC Packings). Using a column-switching technique mediated by a Switchos module (LC Packings), 1 pmol of the digested proteins was loaded onto a 300 μ m i.d. \times 5 mm C18, PepMap nano RP trapping column to preconcentrate and wash away excess salts. The loading solvent containing 0.1% formic acid (pH = 2.9) was flowed at 30 μ L/min. Reverse-phase separation was performed on a 75 μ m i.d. \times 15 cm C18, PepMap nanoseparation column. Eluent A (95% water, 5% acetonitrile, and 0.1% formic acid) and eluent B (5% water, 95% acetonitrile, and 0.1% formic acid) were used to form the gradient. The ESI and MS/MS spectra were recorded in the centroid mode.

All mass spectra were acquired in the positive ion mode. The fraction of peptide modified was determined from the ratio of the area under ion signals for the oxidized radiolytic products to the sum of those for the unoxidized peptides and the oxidized radiolytic products. The oxidized radiolytic products include +14, +16, +32, and +48 Da species relative to the unmodified ions. The fraction of unmodified peptide determined from the multiple experimental repeats versus exposure times (a "dose-response" plot) was fitted

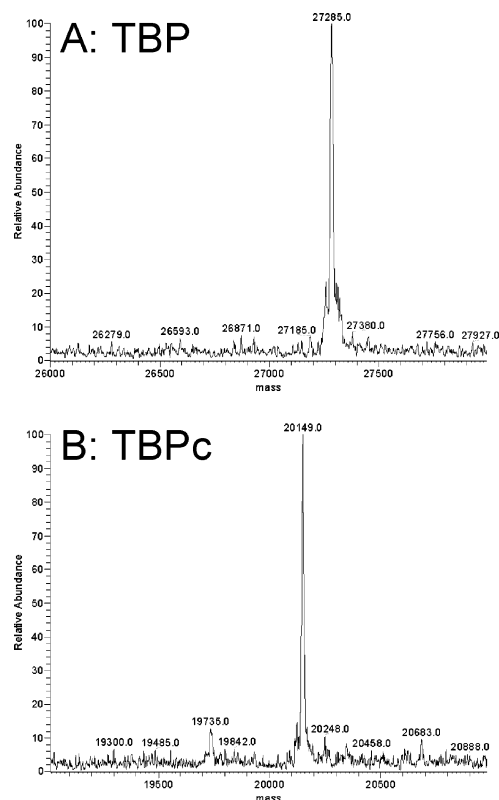


FIGURE 1: Mass spectra of the purified *S. cerevisiae* TBP (A) and TBPc (B) used in these studies obtained using a Thermo Finnigan LCQ classic mass spectrometer using electrospray ionization.

globally to a single exponential decay function with Origin version 6.1 (OriginLabs) to determine the rate of peptide modification. The reported errors of the rate data were determined by the Origin program using 95% confidence limits of the fitting results.

Solvent Accessibility Calculations. The solvent accessibility of individual side chains in the yeast TBP core domain and the DNA-bound form was determined from the PDB coordinate file 1YTB after removing either only TFIIA or TFIIA and the DNA. The program GETAREA 1.1 (http://www.scsb.utmb.edu/cgi-bin/get_a_form.tcl) was used to calculate the solvent-accessible surface area per residue from the PDB files. The amino acid side chains whose solvent accessibilities (see Experimental Procedures) are $\geq 20 \text{ \AA}^2$ are underlined in Table 2 of the Supporting Information.

RESULTS

TBPc and TBP Characterization. Yields of approximately 2.1 mg and 1.3 mg/g of cells were obtained for *S. cerevisiae* TBP and TBPc, respectively. The molecular masses determined by mass spectrometry are 27286 and 20150 Da for TBP and TBPc, respectively (Figure 1). These values compare with molecular masses of 27285 and 20149 Da calculated for these proteins from their sequence. The protein preparations used in this study were >95% homogeneous. TBP contains six tyrosines and no tryptophan in its C-terminal core domain and one tryptophan and no tyrosines in the N-terminal domain. The single tryptophan in the N-terminal domain provides a clear optical signature distinguishing TBPc from TBP (13, 15). The UV absorption and fluorescence emission spectra of our preparations of TBPc and TBP are those expected for proteins without and with

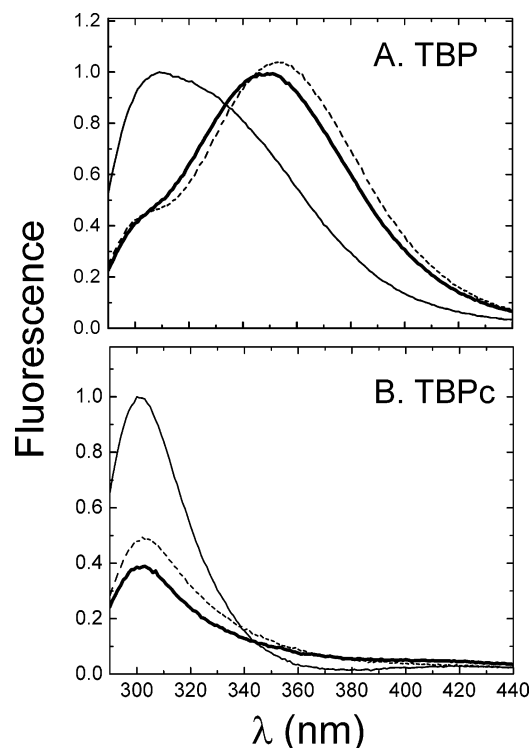


FIGURE 2: Normalized fluorescence emission spectra of *S. cerevisiae* TBP (A) and TBPc (B) native (—) and in buffer containing 8 M urea (---) obtained as described in Experimental Procedures. The bold lines depict the native proteins complexed with DNA.

tryptophan, respectively (Figure 2 and Supporting Information, Figure 1).

The absorption spectra of denatured TBP and TBPc resemble the spectra of the model compounds *N*-acetyl-L-tyrosine and *N*-acetyl-L-tryptophan ethyl esters, demonstrating complete solvent exposure of the aromatic amino acids (data not shown). The spectra of the native proteins are red shifted with higher extinction coefficients consistent with the burial of the aromatic acids in the interior of the proteins (Supporting Information, Figure 1). Consideration the spectral differences between the denatured and native proteins allowed calculation of accurate extinction coefficients (Supporting Information, Table 1) and thus accurate total protein concentrations.

Upon excitation at 275 nm, the 40 nm red shift in the fluorescence emission spectra of TBP observed upon denaturation of the protein contrasts with the invariance of the fluorescence emission spectra of TBPc upon its denaturation (Figure 2, solid and broken lines). Only the quantum efficiency of TBPc decreases. The emission maximum of TBPc also does not change upon DNA binding; only the quantum efficiency decreases (Figure 2B, bold line). Thus, the red shift observed upon the binding of TBP to DNA is entirely due to the single tryptophan present in the N-terminal domain (Figure 2A, bold line).² The presence of Brij, DTT, or both in the solution has no discernible effect on the absorption or fluorescence spectra of TBP and TBPc (unpublished data).

Specific DNA-Binding Activity. We took advantage of the tyrosine fluorescence quenching and tryptophan fluorescence

² This conclusion is confirmed by the comparable red shift and increase in the fluorescence quantum yield observed upon excitation of TBP at 295 nm (data not shown).

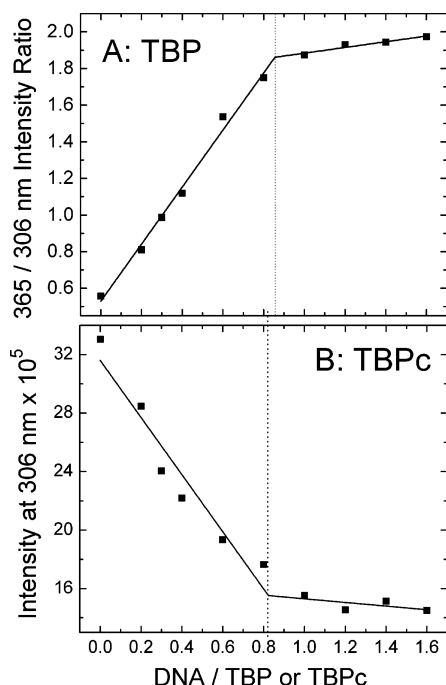


FIGURE 3: Specific DNA-binding activity of a representative preparation of *S. cerevisiae* TBP (A) and TBPc (B) used in these studies. TBP or TBPc at a concentration of 0.5 μM was titrated with increasing concentrations of the 18 bp duplex bearing the sequence TATAAAAG as described in Experimental Procedures. The solid lines are the best fit of two intersecting lines used to determine the equivalence point of the titration (···). The ratio of 365 to 306 nm fluorescence intensity (A, TBP) or fluorescence intensity at 306 nm (B, TBPc) was monitored.

enhancement that occurs upon TBP–DNA complex formation and tyrosine fluorescence quenching upon TBPc–DNA complex formation to accurately and precisely determine the specific DNA-binding activity of preparations of the two proteins (Figure 3). The opposite changes in the fluorescence intensity are due to the enhancement of the tryptophan fluorescence in TBP and the quenching of the tyrosine fluorescence in TBPc (Figure 2). The specific DNA binding activity of both proteins in this example is $\sim 80\%$. Specific activity values ranged from 80% to 100% for the protein preparations used in this study. The reported protein concentrations have been corrected for the activity value determined for the particular protein preparation used in the experiments.

Self-Association. Confirmation that the nonionic detergent Brij-58 present at a concentration of 0.01% in the assay buffer did not affect TBP self-association was obtained by sedimentation equilibrium analysis. Data obtained at two KCl concentrations in the presence and absence of the detergent was best fit by the well-documented monomer–tetramer–octamer assembly model (14, 21) with association free energies indistinguishable from those previously published (Table 1). TBPc dimerizes as previously reported (22, 43) in the absence and presence of Brij-58 although dimerization is weakened by the detergent (Table 1 and Supporting Information, Figure 2). On the basis of the assembly constants, TBP and TBPc are monomeric at the concentrations present in the binding assays presented below that were conducted in solutions containing the detergent. TBP is monomeric in both the presence and absence of the detergent at the higher protein concentrations used in the protein

Table 1: Sedimentation Equilibrium Analysis of TBP and TBPc Self-Association

buffer	initial [TBP] (μM)	$M \leftrightarrow T^a$	$M \leftrightarrow O^a$
from ref 14	0.8–16	ND ^b	-49.3 ± 1.4
TBP	6.6–33	-21.2 ± 0.8	-51.7 ± 1.1
TBP (Brij-58)	6.6–33	-22.2 ± 0.3	-51.7 ± 0.5
buffer	initial [TBPc] (μM)	M_w^c	$M \leftrightarrow D^d$
TBPc	11.0–42	39839 ± 1650	
TBPc (Brij-58)	11.0–42	35745 ± 2063	-7.2 ± 0.7

^a Results shown are the best fit values to the monomer–tetramer–octamer model in the 100 mM KCl assay buffer. Values are ΔG° in kcal/mol. ^b Tetramer was not discernible (ND) in these experiments. ^c The weight-average molecular weight assuming a homogeneous monodisperse particle. ^d Results shown are the best fit values to the monomer–dimer equilibrium. Values are ΔG° in kcal/mol.

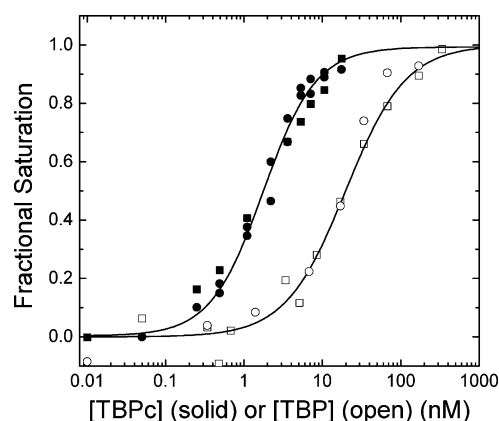


FIGURE 4: Representative set of TBP and TBPc binding isotherms obtained as described in Experimental Procedures. This experiment was conducted in sodium cacodylate buffer containing 0.01% Brij. TBPc (solid symbols) and TBP (open symbols) were bound to the DNA containing the AdMLP (TATAAAAG, circles) or U6 (TATAAATA, squares) promoter TATA box sequences. Global fitting of each set of data to the Hill equation yielded $K_d = 1.8 \pm 0.2$ nM and $n_H = 1.1 \pm 0.1$ and $K_d = 20.0 \pm 2.9$ nM and $n_H = 1.0 \pm 0.1$ for TBPc and TBP, respectively.

Table 2: Affinity Calculated from Paired TBP and TBPc Equilibrium Binding Isotherms for Binding to the AdMLP TATA Box Sequence TATAAAAG

buffer ^a	protein	K_d (nM)	n_H
cacodylate–Brij	TBP	20.0 ± 2.9	1.0 ± 0.1
	TBPc	1.8 ± 0.2	1.1 ± 0.2
KH ₂ PO ₄ –Brij	TBP	$7.7 \pm (-0.4, +0.3)$	1.06 ± 0.04
	TBPc	2.2 ± 0.1	1.06 ± 0.07
KH ₂ PO ₄	TBP	$7.6 \pm (-0.4, +0.3)$	1.02 ± 0.03
	TBPc	2.2 ± 0.1	1.04 ± 0.08
KH ₂ PO ₄ –5% glycerol	TBP	7.2 ± 0.3	1.05 ± 0.04
	TBPc	0.40 ± 0.06	1.06 ± 0.07

^a The buffer is the solution described in Experimental Procedures with the indicated buffering component and additives.

footprinting studies. In these experiments, TBPc is monomeric in the Brij-containing buffer and predominantly dimeric in its absence.

Equilibrium Binding. TBPc binds to TATA box containing DNA with significantly greater affinity than TBP (Figure 4, Table 2). The isotherms obtained for both proteins are well described by the single-site binding polynomial, confirming that coupled equilibria do not contribute to either reaction under these experimental conditions. TBPc always binds with higher affinity although there are subtle variations among

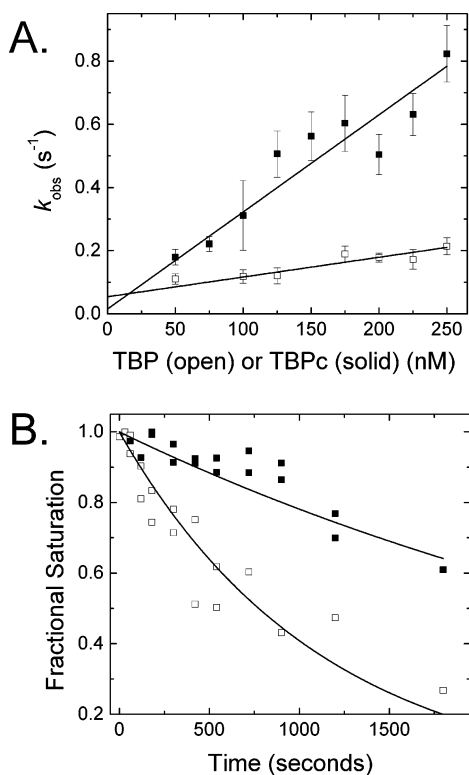


FIGURE 5: (A) Association of TBPc (solid symbols) and TBP (open symbols) to DNA bearing the AdMLP TATA box followed by quench-flow DNase I footprinting. The solid lines depict the best fit of $y = k_a(x) + k_d$ (72) with k_d fixed at the values determined from panel B and $k_a = (6.3 \pm 1.0) \times 10^5$ and $(30.7 \pm 2.0) \times 10^5 \text{ M}^{-1} \cdot \text{s}^{-1}$ for TBP and TBPc, respectively. (B) Dissociation of TBPc (solid symbols) and TBP (open symbols) from DNA bearing the AdMLP TATA box followed by DNase I footprinting. The solid lines depict exponential decay curves with the best fit values of $k_d = (8.9 \pm 0.5) \times 10^{-4}$ and $(2.5 \pm 0.2) \times 10^{-4} \text{ s}^{-1}$ for TBP and TBPc, respectively. The experiments were conducted as described in Experimental Procedures in buffer containing 0.01% Brij.

the several solution conditions tested (Table 2). For example, phosphate is inhibitory of TBP but not TBPc binding. Conversely, glycerol facilitates TBPc binding but has no effect on TBP. Lastly, 0.01% Brij has no effect on the binding of either protein.

DNA Binding Kinetics. The second-order rate constant for TBPc binding to the AdMLP TATA box sequence is 5-fold greater than that determined for TBP (Figure 5A). The linear dependence of k_{obs} on TBP or TBPc concentration is consistent with the simple bimolecular association previously detected by DNase I footprinting for TBP (30). The rates of dissociation of TBP and TBPc also differ. The TBPc–TATA complex is three and one-half times more stable than the TATA complex of the full-length protein (Figure 5B). Thus, the higher affinity of TBPc reported in Figure 5 is a composite of the protein's increased rate of association and decreased rate of dissociation relative to TBP. The association and dissociation progress curves are adequately described by single exponentials under these experimental conditions (data not shown; Figure 5B). It should be noted that these curves reflect an average rate constant and do not provide information about the reaction intermediates that have been visualized by more comprehensive and precise kinetics studies detected by fluorescence resonance energy transfer of dye-labeled DNA (44).

Protein Footprinting. Samples of TBP, TBPc, and their complexes with DNA were exposed to white synchrotron X-ray radiation for 0–150 ms. The relative abundance of unmodified and oxidized tryptic peptide ions was calculated from the ion chromatogram peak area corresponding to the mass of the selected peptide as described in Experimental Procedures. To ensure that the native protein was probed, quantitation of the loss of unmodified peptides was monitored. Oxidation as a function of X-ray exposure was consistently first order (data not shown; ref 39).

The oxidation rate constants for the identified tryptic peptides and comparisons between free and DNA-bound TBP and TBPc are summarized in Figure 6 and Table 2 of the Supporting Information. Representative chromatogram, tandem mass spectra, and the dose–response plot are shown in Supporting Information, Figures 3–5. Differences between the TBP results obtained herein and in previous work conducted under different experimental conditions (18) are addressed in the Discussion. Studies were also conducted in the presence or absence of the nonionic detergent Brij to explore its structural consequences and match the experimental conditions of the biochemical studies presented in Figures 2–5.

The interpretation of the footprinting results is aided by viewing the structural disposition of the oxidized tryptic peptides (Figure 7). The C-terminal domain (TBPc) consists of two subdomains, H2 and H2', that form a continuous, 10-stranded, slightly curved antiparallel β -sheet defining the distinct concave DNA binding saddle (Figure 7E). The loops that emerge from the ends of the saddle between strands S2 and S3 and strands S2' and S3' (the “stirrups”) define a cylindrical cleft. Helices H2 and H2' are cradled on the convex surface of the sheet; the short helices H1 and H1' precede strands S2 and S2' in the primary sequence. The S1 strand connects the N-terminal polypeptide to the H2' helix.

Approximately 60% of the primary sequence is covered by the observed tryptic peptides in the total ion ESI-MS chromatograms. The observed peptides include segments of the N-terminal domain, the DNA binding saddle, and the top side of the C-terminal domain. The X-ray doses used were sufficient to detect modification of reactive aromatic side chains with predicted solvent accessibilities $>40 \text{ \AA}^2$ (data not shown). This limit is slightly greater than the oxidation detection reported in other studies for aromatic side chains with $>20 \text{ \AA}^2$ accessibility (18, 39, 45–48). Detectable peptides with oxidation rate constants $>2 \times 10^{-4} \text{ s}^{-1}$ are considered “unreactive” (Figure 6 and Supporting Information, Table 2). Tandem mass spectrometry (MS/MS) was performed as necessary to confirm the identity of tryptic peptides and/or determine the site (or sites) of oxidation (45, 49). The order of side chain reactivity to oxidation by $\cdot\text{OH}$ is Cys, Met, Phe, Tyr, Trp, Pro, His, and Leu (45, 49). The observed $\cdot\text{OH}$ reactivity depends upon both the intrinsic reactivity of the residues and their solvent accessibility (45, 49, 50). In order to separate out the solvent accessibility dependence of the observed oxidation rate, comparisons of *relative* reactivity changes, such as the presence or absence of the N-terminal domain or DNA binding, are the focus of our study. While the solvent accessibility calculated from a crystal structure is often comparable to the $\cdot\text{OH}$ reactivity in solution, differences have been noted (45).

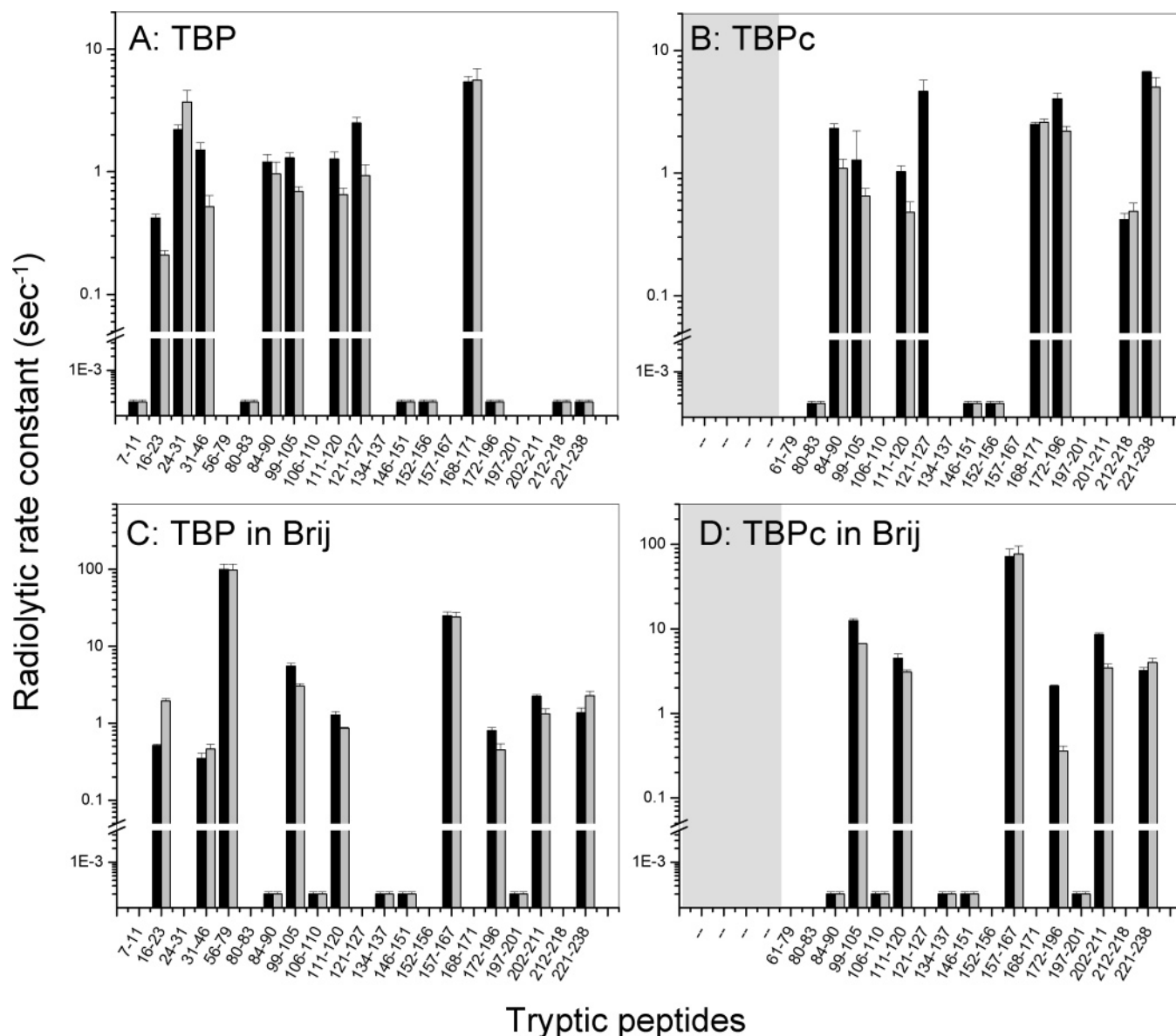


FIGURE 6: Summary of the peptide oxidation rates obtained from the $\cdot\text{OH}$ protein footprinting comparison of TBP and TBPc as described in Experimental Procedures. The black bars are free proteins. The gray bars are TBP or TBPc in an equimolar complex with the TATA box containing DNA oligonucleotide. Peptides not detected by mass spectrometry are not shown. The peptides that are detectable but whose rate constant is $< 2 \times 10^{-5} \text{ s}^{-1}$ are indicated along the bottom of the histograms; these peptides are referred to as unreactive.

The N-Terminal Domain of TBP. The most N-terminal detectable tryptic peptide is 7–11, which contains the reactive residues Leu and Phe. That this peptide is not oxidized in either free TBP or the TBP–DNA complex indicates that the terminus of the N-terminal polypeptide is inaccessible to solvent. In contrast, the next three peptides in the sequence are generally reactive (Figures 6A and 7A). The rate constants of 0.42 and 1.5 s^{-1} measured for peptides 16–23 and 32–47, respectively, are consistent with their reactive residues being solvent accessible. DNA binding changes the reactivity of these three oxidized peptides by ≥ 2 fold. The reactivity of peptide 24–31 increases while those flanking are protected, suggesting that the ends of the N-terminal domain become less accessible while the middle becomes more accessible upon TBP–DNA complex formation (Figures 6A and 7B). Peptide 24–31 contains the sole Trp residue present in TBP and has been the subject of parallel fluorescence investigations (Figure 2 and ref 51).

The H2 Subdomain of TBP and TBPc. Four of the seven detectable peptides in the H2 subdomain (residues 61–160) are significantly and comparably oxidized in TBP and TBPc. The peptides are also comparably protected by DNA in both proteins. The other three peptides of this subdomain are not oxidized in the absence or presence of DNA (Figure 6A,B). The detected peptides include part of the S1 strand, S2–S5 strands, H2 and H1 helices, and the loops joining these secondary folds (Figure 7A,E). The peptides include residues within the DNA binding saddle region (99–105, 111–120, and 121–127) that are protected by ≥ 2 -fold upon DNA binding (Figure 7B,F). These results are consistent with the decrease in solvent accessibility of the probed residues

³ A new analytical method (41) not available during our earlier study (18) allows useful information to be extracted from the methionine-containing peptides 99–105 and 121–127.

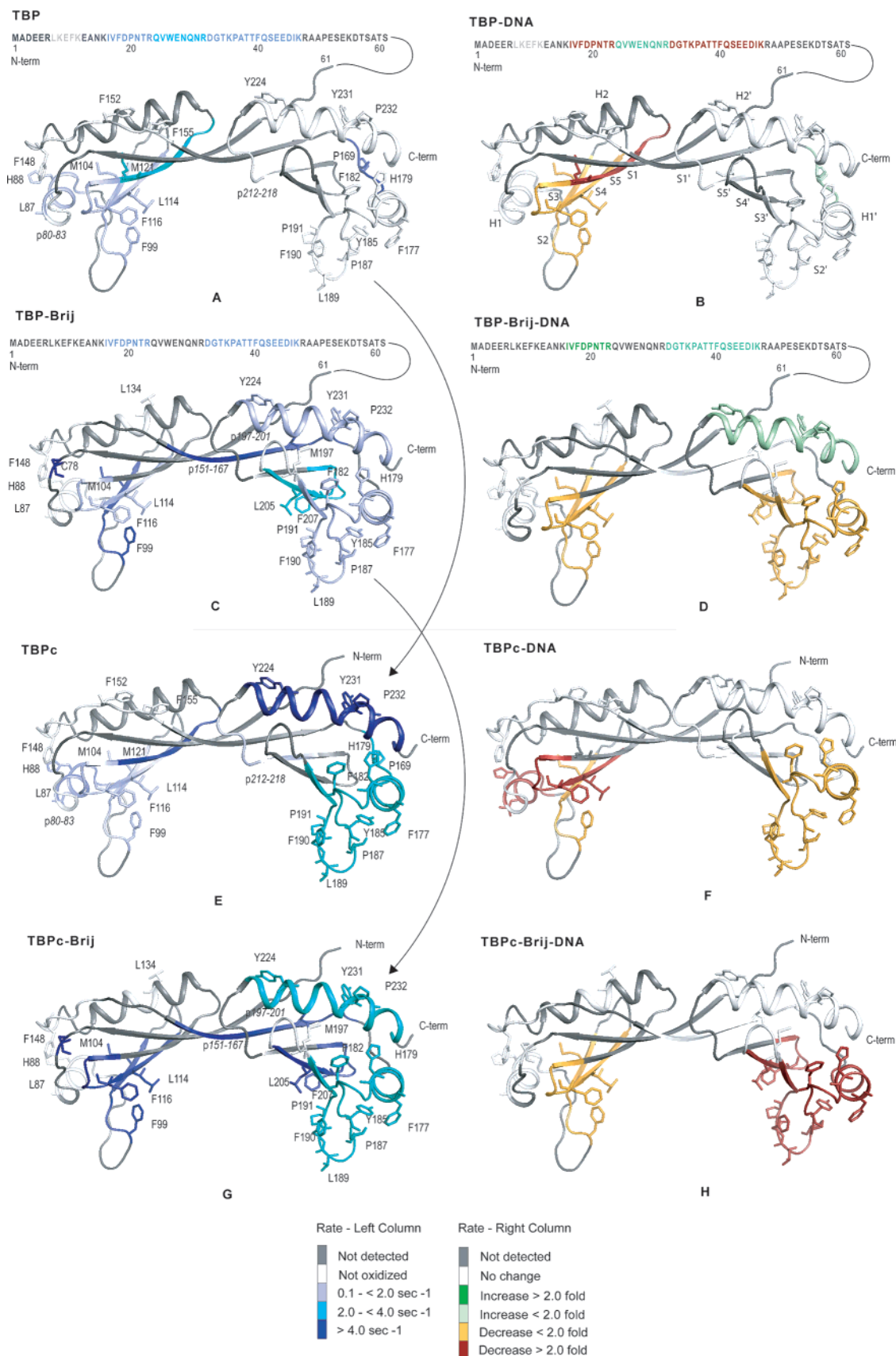


FIGURE 7: Mapping of the tryptic peptides detected by $\cdot\text{OH}$ protein footprinting onto the atomic resolution three-dimensional structure of TBPc (8). The known structure of TBPc is schematically represented with ribbons with the potentially reactive residues having solvent accessibility $\geq 20 \text{ \AA}^2$ (except for Met) displayed as sticks. The side chain color exactly matches its corresponding backbone color. The N-terminal domain is represented by sequence since its atomic resolution structure has not been solved. Panels A–D depict TBP free and DNA bound in the presence and absence of the nonionic detergent Brij. Panels E and H depict the same set of results for TBPc. At the base of each column is a color legend. The left column depicting free protein is colored by relative oxidation rate. The right column depicting the protein complexes with DNA is colored by the relative reactivity change measured upon ligation.

calculated from the TBPc crystal structures.³ Peptide 121–127 was not recovered for the TBPc–DNA complex for reasons unknown.

Peptide 84–90 is of interest since its reactive residues, Leu87 and His88, are situated within the H1 helix on the outside of the proteins and its reactivity decreases ~2-fold in TBPc upon the binding of DNA (Figures 6B and 7F). The reactivity of this peptide does not significantly change in TBP (Figures 6A and 7B). Two peptides (146–151 and 152–156) also situated on the top of the domain are not detectably oxidized in either free or DNA-bound TBP and TBPc (Figures 6A,B and 7A,B,E,F). Since these peptides possess highly reactive Phe residues whose solvent accessibilities are appreciable in the crystal structures, their lack of reactivity suggests that this region is less accessible in solution than predicted by the crystal structures. These results indicate that the solvent-accessible surface of the H2 subdomain is minimally affected by the N-terminal domain. Thus, the reactivity changes observed upon DNA binding are due to an alternative mechanism.

The H2' Subdomain of TBP and TBPc. The H2' subdomain encompasses residues 160–~239 (S1', H1', S2'–S5', and H2'). In contrast to the H2 subdomain, the reactivity of three of the four H2' peptides differs dramatically between TBP and TBPc; peptides 172–196, 212–218, and 221–238 are highly reactive in TBPc (Figures 6B and 7E) and virtually unreactive in TBP (Figures 6A and 7A). These differences in oxidation rate are of greater magnitude than the changes observed upon DNA ligation (Figure 7B,F). Only peptide 168–171 is reactive in both proteins. Unfortunately, a report of the saddle in this subdomain is unavailable due to the absence of peptide 202–211 at this experimental condition.

These results show that the N-terminal domain docks against the H2' subdomain. The extreme protection of peptide 172–196 is notable as it possesses multiple reactive side chains with solvent accessibilities $\geq 40 \text{ \AA}^2$ (Supporting Information, Table 2). Peptide 172–196 includes residues in the H1' subdomain that are outside of the DNA-binding region, S2' and S3', and associated loops in the saddle (Figure 7A,E). Peptide 212–218 is more specific as it possesses a single reactive residue, Leu214, that resides near the DNA-binding saddle. While this peptide is unoxidized in both free TBP and the TBP–DNA complex (Figures 6A and 7A,B), it is reactive in TBPc and 2-fold protected in the TBPc–DNA complex (Figures 6B and 7E,F). This reactivity pattern is consistent with the N-terminal domain binding within the saddle and being displaced upon DNA binding although it remains bound to other surfaces of the H2' subdomain.

A Nonionic Detergent Affects the Structures of TBP and TBPc. Detergents are often used in the study of transcription owing to their stabilization of the constituent factors. Since our binding studies utilize the nonionic detergent Brij (Figures 4 and 5; refs 52 and 53), additional protein footprinting studies were conducted to explore its effect on the structures of TBP and TBPc. Some tryptic peptides observed in the above-described studies are not present and vice versa (compare Figures 6A,C and 6B,D). This effect appears to be due to interaction of the detergent with the chromatography matrix and altered ionization of efficiencies of the peptides or alterations of the digestion efficiencies at specific sites due to the presence of detergents (Supporting

Information, Table 2). However, a sufficient number of common peptides are observed to allow direct comparison between the two conditions. Generally, higher reactivity rates are observed in the presence of the detergent (Figure 6C,D).

The changes in the $\cdot\text{OH}$ reactivity pattern of the N-terminal domain induced by Brij suggest that structural changes are induced by the detergent (Figure 6A,C). While Brij induces a small increase in the modification rate of peptide 16–23 in the free protein, DNA binding *increases* the modification rate by 4-fold compared to the 2-fold rate *decrease* measured in the absence of detergent. Peptide 32–47 behaves similarly. These differences reflect large and *opposite* changes in solvent accessibility of this region in the absence and presence of the detergent.⁴

The $\cdot\text{OH}$ reactivity of TBPc and the core domain of TBP is the same when Brij is present. For example, peptides 197–201 and 202–211 show comparable low and high oxidation rates, respectively, in both proteins (Figures 6C,D and 7C,G). In contrast, extensive protection of TBP's H2' subdomain in the absence of detergent was presented above. We conclude from these data that the H2' subdomain of TBP is protected by the N-terminal domain and Brij inhibits this interdomain interaction. The effect of Brij is most dramatic for the peptides derived from the top side of the H2' subdomain of TBP. Peptides 172–196 and 221–238 are detected under both solution conditions. They are unreactive in the absence of detergent and highly reactive in its presence (compare Figures 6A,C and 7A,C; see Supporting Information, Table 2).

Observed in the Brij experiments is peptide 202–211, which reports on the accessibility of the H2' side of the DNA-binding saddle. This peptide and those reporting on the H2 side of the saddle (peptides 99–105 and 111–120) display comparable 2-fold protections on DNA binding in both TBP and TBPc (Figure 7D,H and Supporting Information, Table 2). The uniform response to DNA binding across the saddle suggests that the N-terminal domain does not occlude this surface in the presence of detergent. Peptide 172–196, spanning the H1' helix and both sides of the saddle, behaves similarly (Figures 7D,H). We conclude that the N-terminal domain is less interactive with the core domain in the presence of Brij compared with its absence.

DISCUSSION

The central role played by TBP in the transcription of eukaryotic genes necessitates a thorough exploration of its structure and function if accurate molecular models of its assembly and function with the other components of the transcription machinery are to be generated. Our understanding of the C-terminal DNA-binding domain of TBP has been aided by its high conservation. In contrast, the role played by the N-terminal domain is ill-defined due in part to its variability among species; its structural diversity may reflect comparable diversity of function.

Tighter TATA Box Binding by TBPc. Quantitating the consequences of its absence is an important step in defining

⁴ Peptide 56–79, which contains a Cys78, is very reactive in both TBP and the TBP–DNA complex, consistent with its predicted solvent accessibility in the X-ray crystal structure. However, this peptide's absence from the mass spectra in the absence of detergent and the absence of peptide 61–79 from the TBPc mass spectra prevent further interpretation of this observation.

the role of the N-terminal domain in TBP function and transcription initiation. A conclusive answer to this question has been hampered by TBP and TBPC self-association and uncertainty in the specific DNA binding activity of protein preparations between which comparisons were made. Subtle changes to the growth conditions and use of a cleavable His-tag expression vector resulted in reproducibly high yields of highly activity protein (Figure 3). Use of protein preparations of defined and high specific activity demonstrates that TATA box binding by the C-terminal domain is inhibited by the presence of the N-terminal domain. The binding affinity difference between TBP and TBPC for the TATA box is as large as an order of magnitude in direct comparisons under identical experimental conditions (Figure 4). A smaller differential is observed in studies utilizing a 14 bp oligonucleotide, suggesting a contribution by the DNA flanking the TATA box to the difference observed by footprinting (51).

Multiple Mechanisms of N-Terminal Domain Modulation of DNA Binding by TBP. The higher affinity of TBPC for the TATA box sequence is consistent with our proposal that the N-terminal domain binds to the DNA-binding saddle and thus competes with the DNA (18). However, the present protein footprinting results (see below) and comparison of the kinetics of TBP and the TBPC TATA box binding suggest that this explanation is incomplete. While the greater rate of TBPC association is consistent with our proposal, its lesser dissociation rate is not (Figure 5). The expectation is for identical TBPC and TBP dissociation rates if the sole effect of the N-terminal domain was to compete with DNA for the saddle. That this is not the case suggests that modulation of TATA box binding by TBP involves processes in addition to competition between DNA and the N-terminal domain for the surface of the saddle. The possibility that the N-terminal domain directly contacts the DNA is opposed by other structural studies (51). Changes in the structure of the C-terminal domain upon deletion of the N-terminal polypeptide is considered at the end of the discussion (51).

Comparing Previous and Present Protein Footprinting Studies of TBP. Protein $\cdot\text{OH}$ footprinting reports on the solvent accessibility of reactive amino acid side chains (54); the spatial resolution of our previous (18) and present studies is at the level of oxidized tryptic peptides. The previous $\cdot\text{OH}$ protein footprinting studies of TBP and the TBP–DNA complex were conducted at lower ionic strength than the present work and in the absence of Mg^{2+} and Brij (18). Also, TBPC was not analyzed in the previous study.

The previous and present (in the absence of Brij) protein footprinting studies of TBP generally agree with several exceptions. Our use of methionine amide to quench secondary oxidation reactions after sample X-ray exposure (55, 56) allows methionine to be used as a structural probe (for example, peptide 99–105; Figure 6) since the loss of unmodified peptide products containing this residue follows an apparent first-order decay (data not shown). Thus, structural information from this peptide is new. We note that the modification rates of some C-terminal domain peptides containing solvent-exposed aromatic amino acids were less than previously measured. This reduced reactivity may result from either alternate side chain orientations or decreased postexposure secondary oxidation reactions (57, 58).

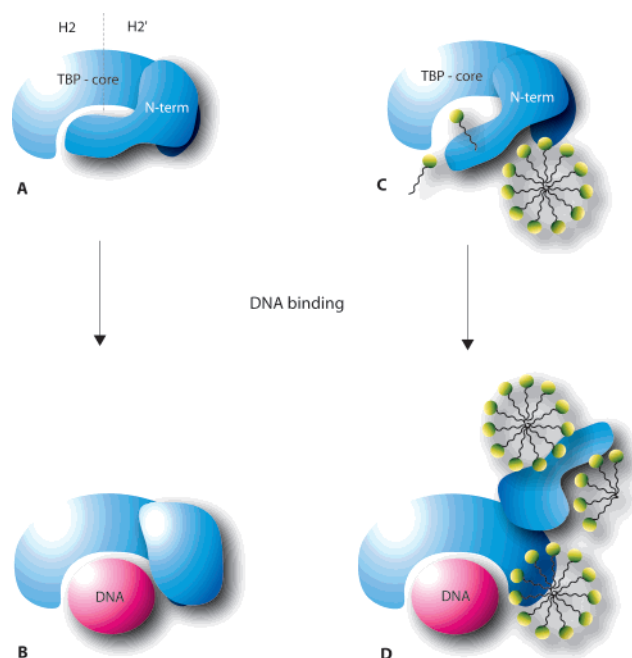


FIGURE 8: Cartoons summarizing our models for the interaction of the N- and C-terminal domains. (A) In the absence of Brij, the N-terminal domain docks into the DNA binding saddle and also binds to the H2' subdomain. (B) When DNA displaces the N-terminal domain from the saddle, its conformation changes, and interaction with the H2' subdomain is perturbed. (C) Interactions between Brij and the protein compete with the interdomain interactions. (D) DNA binding displaces the N-terminal domain. The N-terminal domain does not form a compact structure in the presence of the detergent.

The major $\cdot\text{OH}$ reactivity differences are the helices on the top of the protein and the N-terminal domain. Four peptides in the H2 domain (84–90, 106–110, 146–151, and 152–156) are not oxidized in the present study in either the presence or absence of DNA (Figure 6). Thus, DNA-dependent solvent accessibility changes on the convex side of the H2 domain in TBP observed at low salt are not present in higher salt solution. A similar picture is presented by the convex surface of the H2' domain in contrast to the rate changes previously observed upon DNA binding. Peptide 168–171 remains highly reactive, and peptide 212–218 is not oxidized in both free and DNA-bound TBP. Since the present results are consistent with the solvent accessibility differences calculated from the crystal structures of the core domain, we conclude that the interdomain interaction is reduced in the higher salt solution. As discussed below, the conclusion that there are DNA-dependent changes in the interaction of the C- and N-terminal domains is confirmed although the details of this interaction are different.

Comparing TBPC with TBP. The present study expands upon our previous work (18) in two important ways. First, the analysis of TBPC as well as TBP allows a direct assessment of the N-terminal domain interaction with the core domain. Second, we have analyzed the effect of the commonly used nonionic detergent Brij on TBP structure so that appropriate comparisons with functional data can be made. The footprint of the N- or the C-terminal domain can be directly visualized on Figure 7 (left column) in the presence and absence of Brij by comparing the $\cdot\text{OH}$ reactivity patterns of TBP and TBPC indicated by the arrows along the side of the figure. The N-terminal domain protects the

convex surface of the H2' subdomain as well as both sides of the DNA-binding saddle in both solution conditions, confirming binding of the N-terminal domain to the DNA binding saddle (18). An additional aspect of the interdomain interaction revealed by the present data is that the H2 and H2' sides of the DNA-binding saddle are not symmetrically protected. The greater reactivity changes observed in the H2' subdomain is not unexpected as the N-terminal polypeptide is linked to the C-terminal domain by this subdomain (Figure 7).

Comparison of the TBPc- and TBP-DNA complexes directly shows that the nonionic detergent Brij alters the repositioning of the N-terminal domain upon the binding of DNA (Figure 7, right column). In Brij, the reactivity of the convex surface of the H2' is enhanced in the TBP-DNA complex in contrast to no change in the absence of the detergent (Figure 7, compare panels B and D). Enhancement N-terminal domain reactivity upon DNA binding is also observed in Brij (Figure 7, compare panels B and D). We conclude from these data that the N-terminal domain remains associated with the convex surface of TBP in detergent-free solutions. In contrast there is less interdomain contact (except for the polypeptide connectivity) in the presence of Brij.

These conclusions are summarized in the cartoons shown in Figure 8. Our conclusion is that the N-terminal domain modulates DNA binding and possibly TBP's interactions with general and specific transcription factors that bind to the H2' subdomain. The autoinhibition of DNA binding is reminiscent of that observed for the σ subunit of the prokaryotic RNA polymerase (59–61). This observation establishes a parallel between the regulation of prokaryotic and eukaryotic transcription initiation. That the N-terminal domain remains bound to the convex surface of TBP as well as the saddle suggests autoinhibition of protein binding to this surface in the assembly or regulation of transcription initiation.

Detergent Affects the Structures of both TBP and TBPc. Figures 6 and 7 document a functionally significant change in protein structure induced by Brij, a nonionic detergent, in addition to the above-noted effect on TBPc dimerization (Table 1). These changes contrast with the absence of observed structural changes in bovine serum albumin upon the addition of nonionic detergents at their critical micelle concentrations (62–64). The hydrophobic interaction plays a predominant role in the interaction between proteins and nonionic detergents (62, 63). In contrast, ionic detergents often perturb protein structure significantly (62, 63, 65, 66). The “oil-like” core of the micelle is proposed to solubilize the hydrophobic residues of protein leading to partial or complete unfolding of the native structure (67). The formation of the micelles can also change the solvent structure, thereby altering the solvation properties of a protein (68).

Nonionic detergent-protein interactions are typically weaker than those with ionic detergents (63). However, the nonionic detergent-induced conformation changes in the mutant Bcl-X_L protein have been reported that do not occur with the wild-type counterpart (69). Examples of partial dissociation into subunits of hemoglobin, hemocyanin, and alkaline phosphatase have also been documented (70). Such data demonstrate that nonionic detergents can have unpredictable effects on protein assembly and conformation. Since the DNA-binding saddle of TBP is highly hydrophobic, it is

unsurprising that Brij influences the docking of the N-terminal domain and TBPc dimerization. The inclusion of Brij and similar detergents in assay solutions may thus be less an effect on protein stability and more its minimization of autoinhibitory interdomain interaction.

Conformational Changes within the Domains. The protein footprinting studies described in this paper report on the interaction of the C- and N-terminal domains. An indication of differences in the internal dynamics of the C-terminal domain with and without the N-terminal polypeptide comes from a TBP vs TBPc comparative analysis of the quenching of the intrinsic fluorescence of the tyrosines embedded within the C-terminal core domain together with FRET analysis of DNA bending (15, 51, 71). These studies have shown that the core domain is more compact in TBPc compared to the full-length protein both free in solution and complexed with DNA. The N-terminal domain changes its conformation upon DNA binding, consistent with its repositioning on the C-terminal domain observed herein by protein footprinting (15, 51). The fluorescence studies also show that divalent cations differentially affect the binding of TBPc and TBP to DNA. It is suggested that the N-terminal domain mimics these effects of divalent cations (51), a hypothesis that can be tested by future protein footprinting studies. Together, the fluorescence studies of domain structure and the protein footprinting studies of interdomain interaction support the autoinhibition model shown in Figure 8.

In conclusion, our studies suggest that the N-terminal domain is autoinhibitory to DNA binding and possibly protein-protein interactions by TBP. While multiple mechanisms appear to underlie autoinhibition, the binding of the N-terminal domain to the saddle of the C-terminal core plays a significant role. The first function would reduce nonspecific association of the protein with genomic DNA and thus enhance the specificity of TATA box binding. The latter function may help to orchestrate the sequential assembly of the transcription preinitiation complex. The isomerization that moves the N-terminal domain out of the DNA-binding saddle also exposes the protein-binding surfaces on the top of the C-terminal domain. Thus, isomerization of TBP would ensure that only the TBP molecules that are bound to DNA in productive complexes can assemble the additional factors necessary to initiate transcription.

SUPPORTING INFORMATION AVAILABLE

Five figures and two tables as described in the text. This material is available free of charge via the Internet at <http://pubs.acs.org>.

REFERENCES

- McKnight, S. L. (1996) Transcription revisited: a commentary on the 1995 Cold Spring Harbor Laboratory meeting, “Mechanisms of Eukaryotic Transcription”, *Genes Dev.* 10, 367–381.
- Bondareva, A. A., and Schmidt, E. E. (2003) Early vertebrate evolution of the TATA-binding protein, TBP, *Mol. Biol. Evol.* 20, 1932–1939.
- Nikolov, D. B., Hu, S. H., Lin, J., Gasch, A., Hoffmann, A., Horikoshi, M., Chua, N. H., Roeder, R. G., and Burley, S. K. (1992) Crystal structure of TFIID TATA-box binding protein, *Nature* 360, 40–46.
- Chasman, D. I., Flaherty, K. M., Sharp, P. A., and Kornberg, R. D. (1993) Crystal structure of yeast TATA-binding protein and

- model for interaction with DNA, *Proc. Natl. Acad. Sci. U.S.A.* 90, 8174–8178.
5. Nikolov, D. B., and Burley, S. K. (1994) 2.1 Å resolution refined structure of a TATA box-binding protein (TBP), *Nat. Struct. Biol.* 1, 621–637.
 6. DeDecker, B. S., O'Brien, R., Fleming, P. J., Geiger, J. H., Jackson, S. P., and Sigler, P. B. (1996) The crystal structure of a hyperthermophilic archaeal TATA-box binding protein, *J. Mol. Biol.* 264, 1072–1084.
 7. Kim, J. L., Nikolov, D. B., and Burley, S. K. (1993) Co-crystal structure of TBP recognizing the minor groove of a TATA element, *Nature* 365, 520–527.
 8. Kim, Y., Geiger, J. H., Hahn, S., and Sigler, P. B. (1993) Crystal structure of a yeast TBP/TATA-box complex, *Nature* 365, 512–520.
 9. Kim, J. L., and Burley, S. K. (1994) 1.9 Å resolution refined structure of TBP recognizing the minor groove of TATAAAAG, *Nat. Struct. Biol.* 1, 638–653.
 10. Juo, Z. S., Chiu, T. K., Leiber, P. M., Baikalov, I., Berk, A. J., and Dickerson, R. E. (1996) How proteins recognize the TATA box, *J. Mol. Biol.* 261, 239–254.
 11. Nikolov, D. B., Chen, H., Halay, E. D., Hoffman, A., Roeder, R. G., and Burley, S. K. (1996) Crystal structure of a human TATA box-binding protein/TATA element complex, *Proc. Natl. Acad. Sci. U.S.A.* 93, 4862–4867.
 12. Patikoglou, G. A., Kim, J. L., Sun, L., Yang, S. H., Kodadek, T., and Burley, S. K. (1999) TATA element recognition by the TATA box-binding protein has been conserved throughout evolution, *Genes Dev.* 13, 3217–3230.
 13. Perez-Howard, G. M., Weil, P. A., and Beechem, J. M. (1995) Yeast TATA binding protein interaction with DNA: fluorescence determination of oligomeric state, equilibrium binding, on-rate, and dissociation kinetics, *Biochemistry* 34, 8005–8017.
 14. Daugherty, M. A., Brenowitz, M., and Fried, M. G. (2000) Participation of the amino-terminal domain in the self-association of the full-length yeast TATA binding protein, *Biochemistry* 39, 4869–4880.
 15. Khrapunov, S., Pastor, N., and Brenowitz, M. (2002) Solution structural studies of the *Saccharomyces cerevisiae* TATA binding protein (TBP), *Biochemistry* 41, 9559–9571.
 16. Horikoshi, M., Yamamoto, T., Ohkuma, Y., Weil, P. A., and Roeder, R. G. (1990) Analysis of structure-function relationships of yeast TATA box binding factor TFIID, *Cell* 61, 1171–1178.
 17. Kuddus, R., and Schmidt, M. C. (1993) Effect of the non-conserved N-terminus on the DNA binding activity of the yeast TATA binding protein, *Nucleic Acids Res.* 21, 1789–1796.
 18. Rashidzadeh, H., Khrapunov, S., Chance, M. R., and Brenowitz, M. (2003) Solution structure and interdomain interactions of the *Saccharomyces cerevisiae* “TATA binding protein” (TBP) probed by radiolytic protein footprinting, *Biochemistry* 42, 3655–3665.
 19. Mittal, V., and Hernandez, N. (1997) Role for the amino-terminal region of human TBP in U6 snRNA transcription, *Science* 275, 1136–1140.
 20. Coleman, R. A., and Pugh, B. F. (1997) Slow dimer dissociation of the TATA binding protein dictates the kinetics of DNA binding, *Proc. Natl. Acad. Sci. U.S.A.* 94, 7221–7226.
 21. Daugherty, M. A., Brenowitz, M., and Fried, M. G. (1999) The TATA-binding protein from *Saccharomyces cerevisiae* oligomerizes in solution at micromolar concentrations to form tetramers and octamers, *J. Mol. Biol.* 285, 1389–1399.
 22. Campbell, K. M., Ranallo, R. T., Stargell, L. A., and Lumb, K. J. (2000) Reevaluation of transcriptional regulation by TATA-binding protein oligomerization: predominance of monomers, *Biochemistry* 39, 2633–2638.
 23. Parkhurst, K. M., Richards, R. M., Brenowitz, M., and Parkhurst, L. J. (1999) Intermediate species possessing bent DNA are present along the pathway to formation of a final TBP-TATA complex, *J. Mol. Biol.* 289, 1327–1341.
 24. Jackson-Fisher, A. J., Burma, S., Portnoy, M., Schneeweis, L. A., Coleman, R. A., Mitra, M., Chitikila, C., and Pugh, B. F. (1999) Dimer dissociation and thermosensitivity kinetics of the *Saccharomyces cerevisiae* and human TATA binding proteins, *Biochemistry* 38, 11340–11348.
 25. Adams, C. A., Kar, S. R., Hopper, J. E., and Fried, M. G. (2004) Self-association of the amino-terminal domain of the yeast TATA-binding protein, *J. Biol. Chem.* 279, 1376–1382.
 26. Makrides, S. C. (1996) Strategies for achieving high-level expression of genes in *Escherichia coli*, *Microbiol. Rev.* 60, 512–538.
 27. Pugh, B. F. (1995) Purification of the human TATA-binding protein, TBP, *Methods Mol. Biol.* 37, 359–367.
 28. Georgiou, G., and Valax, P. (1996) Expression of correctly folded proteins in *Escherichia coli*, *Curr. Opin. Biotechnol.* 7, 190–197.
 29. Puglisi, J. D., and Tinoco, I., Jr. (1989) Absorbance melting curves of RNA, *Methods Enzymol.* 180, 304–325.
 30. Petri, V., Hsieh, M., Jamison, E., and Brenowitz, M. (1998) DNA sequence-specific recognition by the *Saccharomyces cerevisiae* “TATA” binding protein: promoter-dependent differences in the thermodynamics and kinetics of binding, *Biochemistry* 37, 15842–15849.
 31. Petri, V., Hsieh, M., and Brenowitz, M. (1995) Thermodynamic and kinetic characterization of the binding of the TATA binding protein to the adenovirus E4 promoter, *Biochemistry* 34, 9977–9984.
 32. Cloutier, T. E., Librizzi, M. D., Mollah, A. K., Brenowitz, M., and Willis, I. M. (2001) Kinetic trapping of DNA by transcription factor IIIB, *Proc. Natl. Acad. Sci. U.S.A.* 98, 9581–9586.
 33. Gill, S. C., and von Hippel, P. H. (1989) Calculation of protein extinction coefficients from amino acid sequence data, *Anal. Biochem.* 182, 319–326.
 34. Edelhoch, H. (1967) Spectroscopic determination of tryptophan and tyrosine in proteins, *Biochemistry* 6, 1948–1954.
 35. Brenowitz, M., and Senechal, D. F. (1989) DNase I footprint analysis of protein-DNA binding, in *Current Protocols in Molecular Biology* (Ausubel, F. M., Brent, R., Kingston, R. E., Moore, D. D., Seidman, J. G., Smith, J. A., and Struhl, K., Eds.) p Unit 12.14, John Wiley and Sons, New York.
 36. Hsieh, M., and Brenowitz, M. (1996) Quantitative kinetics footprinting of protein-DNA association reactions, *Methods Enzymol.* 274, 478–492.
 37. Petri, V., and Brenowitz, M. (1997) Quantitative nucleic acids footprinting: thermodynamic and kinetic approaches, *Curr. Opin. Biotechnol.* 8, 36–44.
 38. Guan, J. Q., and Chance, M. R. (2005) Structural proteomics of macromolecular assemblies using oxidative footprinting and mass spectrometry, *Trends Biochem. Sci.* 30, 583–592.
 39. Gupta, S., Mangel, W. F., McGrath, W. J., Perek, J. L., Lee, D. W., Takamoto, K., and Chance, M. R. (2004) DNA binding provides a molecular strap activating the adenovirus proteinase, *Mol. Cell. Proteomics* 3, 950–959.
 40. Ralston, C. Y., Sclavi, B., Sullivan, M., Deras, M. L., Woodson, S. A., Chance, M. R., and Brenowitz, M. (2000) Time-resolved synchrotron X-ray footprinting and its application to RNA folding, *Methods Enzymol.* 317, 353–368.
 41. Xu, G., and Chance, M. R. (2005) Radiolytic modification of sulfur-containing amino acid residues in model peptides: fundamental studies for protein footprinting, *Anal. Chem.* 77, 2437–2449.
 42. Xu, G., Kiselar, J., He, Q., and Chance, M. R. (2005) Secondary reactions and strategies to improve quantitative protein footprinting, *Anal. Chem.* 77, 3029–3037.
 43. Coleman, R. A., Taggart, A. K., Benjamin, L. R., and Pugh, B. F. (1995) Dimerization of the TATA binding protein, *J. Biol. Chem.* 270, 13842–13849.
 44. Powell, R. M., Parkhurst, K. M., Brenowitz, M., and Parkhurst, L. J. (2001) Marked stepwise differences within a common kinetic mechanism characterize TATA-binding protein interactions with two consensus promoters, *J. Biol. Chem.* 276, 29782–29791.
 45. Kiselar, J. G., Maleknia, S. D., Sullivan, M., Downard, K. M., and Chance, M. R. (2002) Hydroxyl radical probe of protein surfaces using synchrotron X-ray radiolysis and mass spectrometry, *Int. J. Radiat. Biol.* 78, 101–114.
 46. Kiselar, J. G., Janmey, P. A., Almo, S. C., and Chance, M. R. (2003) Structural analysis of gelsolin using synchrotron protein footprinting, *Mol. Cell. Proteomics* 2, 1120–1132.
 47. Kiselar, J. G., Janmey, P. A., Almo, S. C., and Chance, M. R. (2003) Visualizing the Ca²⁺-dependent activation of gelsolin by using synchrotron footprinting, *Proc. Natl. Acad. Sci. U.S.A.* 100, 3942–3947.
 48. Guan, J. Q., Vorobiev, S., Almo, S. C., and Chance, M. R. (2002) Mapping the G-actin binding surface of cofilin using synchrotron protein footprinting, *Biochemistry* 41, 5765–5775.
 49. Takamoto, K., and Chance, M. R. (2006) Radiolytic protein footprinting with mass spectrometry to probe the structure of macromolecular complexes, *Annu. Rev. Biophys. Biomol. Struct.*

50. Maleknia, S. D., Ralston, C. Y., Brenowitz, M. D., Downard, K. M., and Chance, M. R. (2001) Determination of macromolecular folding and structure by synchrotron x-ray radiolysis techniques, *Anal. Biochem.* 289, 103–115.
51. Khrapunov, S., and Brenowitz, M. (2007) Influence of the N-terminal domain and divalent cations on self association and DNA binding by the *Saccharomyces cerevisiae* TATA Binding Protein, *Biochemistry* 46, 4876–4887.
52. Librizzi, M. D., Moir, R. D., Brenowitz, M., and Willis, I. M. (1996) Expression and purification of the RNA polymerase III transcription specificity factor IIB70 from *Saccharomyces cerevisiae* and its cooperative binding with TATA-binding protein, *J. Biol. Chem.* 271, 32695–32701.
53. Sprouse, R. O., Brenowitz, M., and Auble, D. T. (2006) Snf2/Swi2-related ATPase Mot1 drives displacement of TATA-binding protein by gripping DNA, *EMBO J.* 25, 1492–1504.
54. Takamoto, K., and Chance, M. R. (2006) Radiolytic protein footprinting with mass spectrometry to probe the structure of macromolecular complexes, *Annu. Rev. Biophys. Biomol. Struct.* 35, 251–276.
55. Takamoto, K., and Chance, M. R. (2006) Radiolytic protein footprinting with mass spectrometry to probe the structure of macromolecular complexes, in *Annu. Rev. Biophys. Biomol. Struct.*
56. Maleknia, S. D., Ralston, C. Y., Brenowitz, M. D., Downard, K. M., and Chance, M. R. (2001) Determination of macromolecular folding and structure by synchrotron x-ray radiolysis techniques, *Anal. Biochem.*, 103–115.
57. Lasch, P., Petras, T., Ullrich, O., Backmann, J., Naumann, D., and Grune, T. (2001) Hydrogen peroxide-induced structural alterations of RNase A, *J. Biol. Chem.* 276, 9492–9502.
58. Davies, M. J., Fu, S., Wang, H., and Dean, R. T. (1999) Stable markers of oxidant damage to proteins and their application in the study of human disease, *Free Radical Biol. Med.* 27, 1151–1163.
59. Dombroski, A. J., Walter, W. A., and Gross, C. A. (1993) Amino-terminal amino acids modulate sigma-factor DNA-binding activity, *Genes Dev.* 7, 2446–2455.
60. Dombroski, A. J., Walter, W. A., and Gross, C. A. (1993) The role of the sigma subunit in promoter recognition by RNA polymerase, *Cell. Mol. Biol. Res.* 39, 311–317.
61. Dombroski, A. J., Johnson, B. D., Lonetto, M., and Gross, C. A. (1996) The sigma subunit of *Escherichia coli* RNA polymerase senses promoter spacing, *Proc. Natl. Acad. Sci. U.S.A.* 93, 8858–8862.
62. Wasylewski, Z., and Kozik, A. (1979) Protein–non-ionic detergent interaction. Interaction of bovine serum albumin with alkyl glucosides studied by equilibrium dialysis and infrared spectroscopy, *Eur. J. Biochem.* 95, 121–126.
63. Zadymova, N. M., Yampol'skaya, G. P., and Filatova, L. Y. (2006) Interaction of bovine serum albumin with nonionic surfactant Tween 80 in aqueous solutions: Complexation and association, *Colloid J.* 66, 146–152.
64. Toth, G., and Madarasz, A. (2006) Structure of BRIJ-35 nonionic surfactant in water: a reverse Monte Carlo study, *Langmuir* 22, 590–597.
65. Das, T. K., Mazumdar, S., and Mitra, S. (1998) Characterization of a partially unfolded structure of cytochrome c induced by sodium dodecyl sulphate and the kinetics of its refolding, *Eur. J. Biochem.* 254, 662–670.
66. Kim, P. S., and Baldwin, R. L. (1982) Specific intermediates in the folding reactions of small proteins and the mechanism of protein folding, *Annu. Rev. Biochem.* 51, 459–489.
67. Ikeda, S., Ozeki, S., and Hayashi, S. (1980) Size and shape of charged micelles of ionic surfactants in aqueous salt solutions, *Biophys. Chem.* 11, 417–423.
68. Tanford, C. (1980) *The Hydrophobic Effect: Formation of Micelles and Biological Membranes*, John Wiley, New York.
69. Tan, Y. J., and Ting, A. E. (2000) Non-ionic detergent affects the conformation of a functionally active mutant of Bcl-X(L), *Protein Eng.* 13, 887–892.
70. Umbreit, J. N., and Strominger, J. L. (1973) D-Alanine carboxypeptidase from *Bacillus subtilis* membranes. I. Purification and characterization, *J. Biol. Chem.* 248, 6759–6766.
71. Khrapunov, S., and Brenowitz, M. (2004) Comparison of the effect of water release on the interaction of the *Saccharomyces cerevisiae* TATA binding protein (TBP) with “TATA box” sequences composed of adenosine or inosine, *Biophys. J.* 86, 371–383.
72. Johnson, K. A. (1995) Rapid quench kinetic analysis of polymerases, adenosinetriphosphatases, and enzyme intermediates, *Methods Enzymol.* 249, 38–61.

BI7003608